2010 AGU Fall Meeting, San Francisco (CA), 13th December 2010 - Paper Number : S13A-1960

GROUND MOTION POLARIZATION IN FAULT ZONES : RELATION WITH BRITTLE DEFORMATION FIELDS

M. Pischiutta[(1)], A. Rovelli[(1)], J.B. Fletcher[(2)], F. Salvini[(3)], Y. Ben Zion[(4)]

marta.pischiutta@ingv.it, antonio.rovelli@ingv.it, jfletcher@usgs.gov, salvini@uniroma3.it, benzion@ucsd.edu

(1) Istituto Nazionale di Geofisica e Vulcanologia, sezione Roma 1, Via di Vigna Murata 605, 00146, Rome
(2) US Geological Survey, Menlo Park, CA 94025, USA
(3) Università Roma Tre, Department of Earth Sciences, Largo San Leonardo Murialdo 1, 00146, Rome.
(4) University of Southern California, Department of Earth Sciences, Los Angeles, CA 90089-0740, USA

Abstract

Several recent studies indicate that ambient noise and seismic signals in fault zones tend to be polarized on the horizontal plane with a clear and preferred orientation. Here we present a summary of past experiments as well as new study cases showing evidence of this effect. In previous papers, the role of fluid-filled microcracks in the damage zone was hypothesized. We have then explored an hypothesis based on the fracture field orientation in the fault damage zone by applying the package FRAP3 (Salvini, 2002) to model the brittle deformation field expected for the studied faults.

1) Fault brittle deformation models

The damage zone associated to the development of a fault, consists of a brittle deformation zone around both sides of the fault that can reach up to 200 m (Caine, 1996). It is characterized by the presence of cracks (i.e. fracture systems referred also as fracture cleavages or Riedel fracture systems), which show a systematic orientation and are very intensly closely spaced. They are produced by the interaction of the tectonic stress and the near-fault local stress that is caused by the friction and elastic stress accumulation during fault activity (Riedel 1929, Harding 1951, Hobbs et al., 1976). Depending on the local stress tensor and the brittle rheology of the hosting rock (Mandl, 2000), four types of fracture can develop which orientation depends on the direction of the resulting stress localized around the fault:

- extensional fractures (joints)
- synthetic faulting or cleavage (i.e. with movement consistent with the main fault kinematics)
- antithetic faulting or cleavage (i.e. with movement sense opposite to that of the main fault
- pressure solution surfaces.

Synthetic cleavages represent in most cases the most common fracture system that develops in the fault damage zone. In this work we modelled the orientation of fracture fields as well as the probability of each type to develop using the package FRAP 3 (Salvini, 2002).

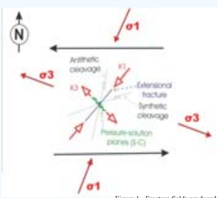

Figure 1 - Fracture fields produced in the fault damage zone by the kinematic stress component.

2) Polarization Analysis

1) Covariance Matrix: Method (Jurkevics 1988) After bandpass filtering signals, the covariance matrix is calculated along a series of partially overlapping time windows applied to the three components of motion. Diagonalization yields eigenvalues λ1>λ2>λ3 and eigenvectors (U1>U2>U3) that allow the definition of the polarization ellipsoid.

For each window we estimate the following parameters:

I *(Incidence)* = arccos(u1)

***R** (Rectilinearity)*= $1-\frac{\lambda_2+\lambda_3}{2\lambda_1}$

***AZ** (Azimuth)* = the angle between the geographic North and the projection of the main eigenvector on the horizontal plane.

***P** (Planarity)* = $1-\frac{2\lambda_3}{\lambda_1+\lambda_2}$

2) Spectral Method: Standard Spactral Ratios - SSRs (Spudich et al., 1996). Rotated Receiver Functions - Rfs

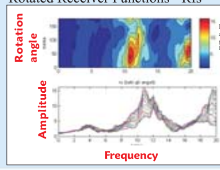

Figure 2 - Spectra calculated for all the angles of rotation and the contours of the geometric mean of spectral ratios as a function of frequency (x axis) and direction of motion (y axis).

Hierarchical criterion

To increase the weight of AZ of time windows with higher degree of rectilinearity and more horizontal motion, values of AZ with R < 0.5 and I < 45° were excluded from statistics. Values of R and I in the intervals 0.5<R<1 and 45°<I<90° are normalized between 0 and 1.
A weight factor WH is obtained from their product which is applied to AZ, producing a weighted version of the rose diagram of polarization. To ensure that the population is large enough to be representative, the percentage of rejected time windows is also checked

Figure 3 - Example of covariance matrix analysis results. Rose diagrams produced by plotting the polarization azimuths (AZ) from the whole set of analyzed time windows (cyan) and by applying the hierarchical criterion (red).The percentage of time windows used is reported as well.

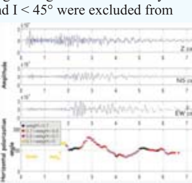

Figure 4 - Polarization angles plotted versus time. The weights associated to each time window are represented though a colour scale (see legend).

3) The Hayward Fault study case

We investigate ground motion polarization in the Hayward fault zone near Niles Canyon, Fremont (CA). Waveforms of 12 earthquakes recorded by a seven accelerometer seismic array around the fault are analyzed, finding a tendency of ground motion to be polarized in the horizontal plane in the vicinity of the fault. In order to verify whether the observed polarization could be ascribed to a source effect, the source polarization was modeled for direct P and S waves using the software ISOSYN (Spudich & Xu, 2003) for the five earthquakes indicated with purple labels in Figure 5. The observed polarization was never consistent with the source expectation, concluding that it is caused by a path or site effect. At two on-fault stations (ND6 and ND7), ground motion polarization is oriented N88°±19° and N83°±32°, respectively. The third on-fault station (ND3) shows a more complex behavior, polarization varying in different frequency bands. However, a similar polarization of N86°±7° is found in the frequency band 6-8 Hz.

Figure 5 - Epicenters of the 12 selected earthquakes. Faults projections are depicted through cyan lines and the array position through a red triangle. In the inset: location of the array installed just across the fault (red line) near Niles Canyon, Fremont.

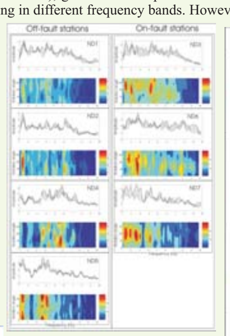

Figure 7 - Mean HVSRs averaged over the selected events. In the upper panels, the heighest spectral ratios for different rotation angles (from 0° to 180°) are shown, while the lower panels represent contour plots versus frequency and direction of motion.

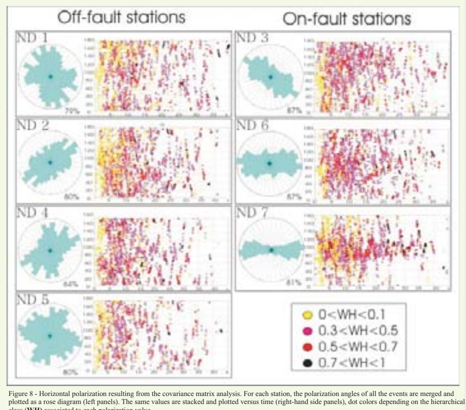

Figure 8 - Horizontal polarization resulting from the covariance matrix analysis. For each station, the polarization angles of all the events are merged and plotted as a rose diagram (left panels). The same values are stacked and plotted versus time (right-hand side panels), dot colors depending on the hierarchical class (WH) associated to each polarization value.

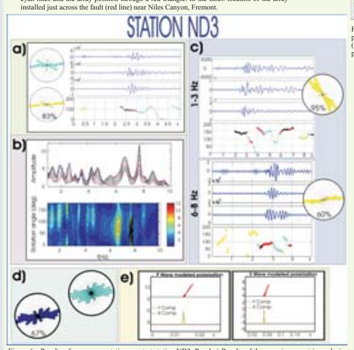

Figure 6 - Results of one representative event at station ND3. Panel a) Results of the covariance matrix analysis (1-7 Hz) polarization values are plotted along the signals with the related rose diagrams.(the cyan one represents all data, the yellow one is obtained applying the weight application). Panel b) HVSRs of ND3. Panel c) Covariance matrix analysis results by differing two frequency bands: 1-3 Hz and 6-8 Hz. Rose diagrams are made by applying the hierarchical criterion. Panel d) Cumulative result of polarization analysis of events #4,5,8,9,10 in the frequency band 6-8 Hz .Panel e) Source polarization modeled for P and S waves for this event.

The fractures orientation (synthetic cleavage) produced by the kinematic stress field in the fault damage zone

The fault was modelled as a 10x2 km surface, with an average N160°E strike and dipping 75°E. The movement was fixed right-lateral strike-slip.

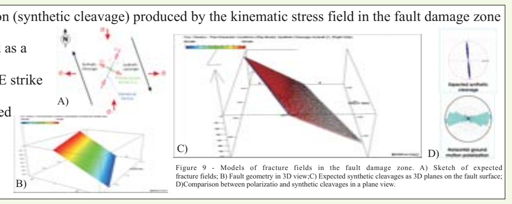

Figure 9 - Models of fracture fields in the fault damage zone. A) Sketch of expected fracture fields; B) Fault geometry in 3D view;C) Expected synthetic cleavages as 3D planes on the fault surface; D)Comparison between polarizatio and synthetic cleavages in a plane view.

An orthogonal relation between polarization and the expected synthetic cleavages is recognized

4) The Pernicana Fault study case

The active Pernicana fault system is one of the most significant tectonic structures of the NE flank of Mt Etna, which also plays an important role in controlling the instability of Etna's eastern flank. Di Giulio et al. (2009) used both microtremors and ambient noise, finding relevant variation of the horizontal polarization on several sites when moving from the fault hanging wall to the footwall in the seismogenic sector outlined in Figure 10, characterized by a sinistral oblique slip kinematics.

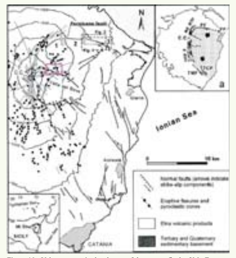

Figure 10 - Volcano-tectonic sketch map of the eastern flank of Mt. Etna (Azzaro 2001) and segment studied by Di Giulio et al. (2009).

A directional effect around 1 Hz is recognized on the rotated receiver functions (Figure 11). Stations installed on the fault hanging wall (# 7, 9, 10, 11, 12 and 13) show a directional effect around N160 in the frequency range 0.7–2 Hz while station installed on fault footwall (#3, 4, 5 and 6) show a predominant polarization direction of about N120 in the same frequency band.

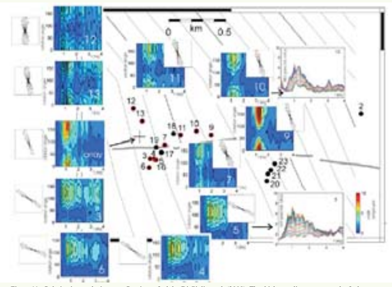
Figure 11 - Polarization analysis across Pernicana fault by Di Giulio et al. (2009). The thick gray line represents the fault trace. HVSR and rose diagrams calculated in the frequency range 1-4 Hz are shown for each measurement site (red circles).

In order to explain the observed variation of polarization azimuth, the brittle deformation in the fault damage zone was analitically computed. The fault was modelled as a 10x2 km surface, with an average E-W strike and dipping 85°S. The rock rheological parameters were fixed as: density 2800 kg/m3, cohesion 5MPs, Poisson ratio of 0.25, Friction angle of 30°, stress drop coefficient 50%, shale content 10% The movement was set left-lateral strike-slip with a total displacement of 200 m. The regional stress field was fixed as:

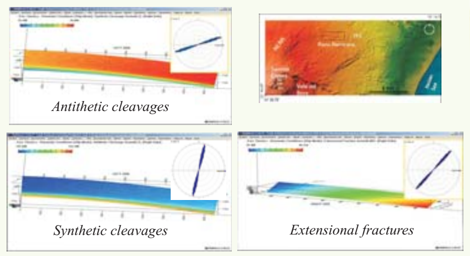

Figure 12 - Modelling of brittle deformation fields in Pernicana fault zone

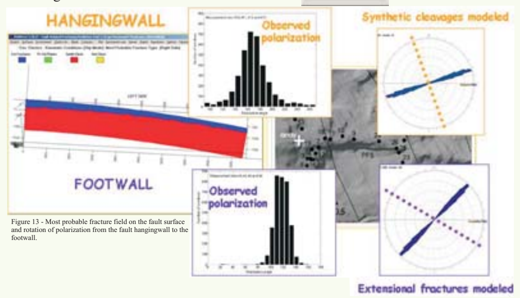

Figure 13 - Most probable fracture field on the fault surface and rotation of polarization from the fault hangingwall to the footwall.

The rotation of polarization azimuth, from N160 to N120 moving from the fault hanging wall to the fault footwall is explained in terms of a differential probability to develop of different brittle deformation fields. The synthetic cleavages (N75) is more diffuse on the fault hangingwall while extensional fractures (N40) dominate the fault footwall footwall. |A perpendicular relation between polarization and the most diffuse fracture field is again recognized.

THE RELATION WITH ANISOTROPY

5) San Andreas fault study case : Parkfield area

Polarization analysis was led out on around 2000 seismic events occurred in 2004 and recorded by the HRSN array. Stations MMNB and GHIB located close to the fault zone found a marked and persistent polarization effect in N85° direction. The comparison with S wave fast component orientation (Boness & Zoback, 2004) revealed a perpendicular relation with anisotropy.

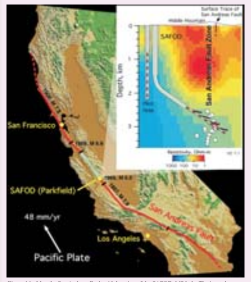

Figure 14 - Map the San Andreas Fault with location of the SAFOD drill hole. The inset shows a sketch of the SAFOD drilling plan of the pilot and main hole superimposed on electrical resistivity structure. Redrawn from http://www.nsf.gov

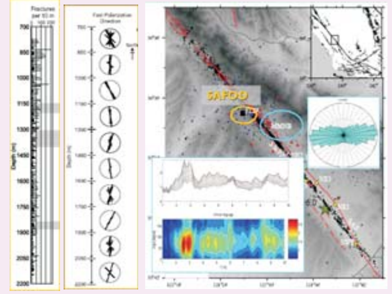

Figure 15 - Map of the Parkfield section of the San Andreas fault (SAF) redrawn from Lewis & Ben Zion (2010). Red lines indicate major faults. The earthquakes used in the analysis (from the relocated catalogue of Thurber *et al,* 2006) are shown as black circles and the epicentre of the 2004 M6 Parkfield event is highlighted as a green star. Polarization analysis results at station MMNB (HVSRs and rose diagram) are plotted as well. On the left, the direction of S waves fast component found by Boness & Zoback (2004) in the SAFOD pilot hole is shown as well.

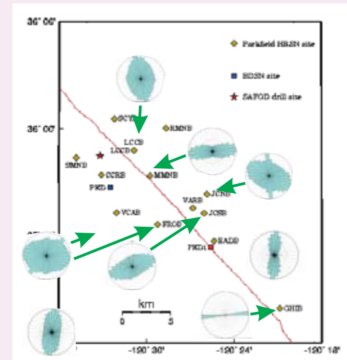

Figure 16 - Cumulative results of polarization analysis performed on the whole data set in the frequency band 1-10 Hz at stations of HRSN array.

A marked polarization effect is observed at stations MMNB and GHIB, close to the San Andreas fault damage zone, along N85° direction Polarization is orthogonal to the mean fast component of S waves velocity found by Boness & Zoback (2004) in the SAFOD pilot hole.

6) Val d'Agri study case

The Agri Valley horsts the largest European on-shore oil field and has been deeply explored by geophysical, seismic and wells. The polarization analysis was carried out on the data set collected in the period May 2005 – June 2006 by Valoroso *et al. (*2009) and among them 22 events were selected with different backazimuth and magnitudes between 0.5 and 2.7.
On this data set Pastori et al. (2009) estimated the fast direction of shear waves velocity using the S waves splitting method.

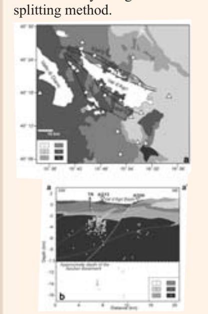
Figure 17 – Panel a) Schematic geological map of the Agri Valley region. (1) Quaternary continental deposits; (2) foredeep and flysch deposits; (3) basinal deposit,clays and slope carbonates; (4) Lagonegro basin limestones; (5) limestones of the Western Platform; (6) limestones of the Apulia Platform.EAFS: Eastern Agri Fault System, MMFS: Monti della Maddalena Fault System. Solid triangles depict seismic stations. Panel b) Schematic vertical cross-section a-a' across the Agri Valley basin (modified after Menardi Noguera & Rea (2000). Redrawn from Pastori *et al.* (2009).

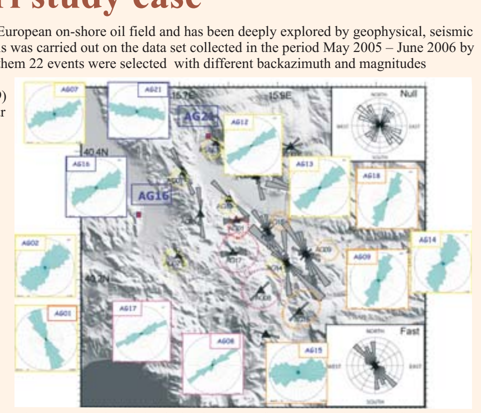

Figure 18 – Orientation of horizontal polarization (cyan rose diagrams) and comparison with the direction of the S-waves fast component found by Pastori *et al.*(2009). The colour around each station is related to the angle between polarization and S wave fast component: yellow=75°<angle<90°, orange=60°<angle<70°; rose=50°<angle<25°; blue=anisotropy data not available.

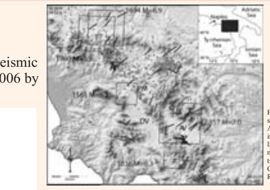
Figure 19 - Topographic map of the southern sector of the Southern Apennines with the historical and instrumental seismicity. The black lines represent the orientation of minimum horizontal stress from s tress indicators (modified after Cucci *et al.* 2004) Redrawn from Pastori *et al.* (2009).

We modelled the brittle deformation fields associated to the most relevant tectonic features in Val d'Agri basin: a dip slip fault with NW-SE strike and dip 70°W. Due to the fault dip-slip kinematic the different fracture fields produced differ only in plunging all showing the same strike.

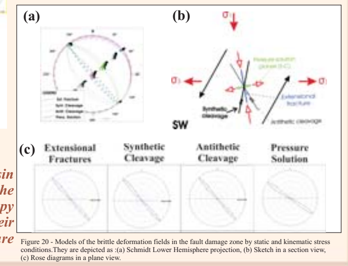

Figure 20 - Models of the brittle deformation fields in the fault damage zone by static and kinematic stress conditions.They are depicted as :(a) Schmidt Lower Hemisphere projection, (b) Sketch in a section view, (c) Rose diagrams in a plane view.

This study performed on a large scale in the Val d Agri extensional basin clearly revealed that polarization occurs in a direction perpendicular to the Vs fast component.Pastori et al.(2009) pointed out that in this area anisotropy is due to fluid-filled cracks. Our models of fracture fields confirmed their conclusion revealing that polarization is also orthogonal to fracture field direction.

7) Paganica fault (L'Aquila) study case

To study polarization across Paganica fault we installed two seismic stations near the fault trace at the surface that recorded ambient noise for 40 minutes on 5 August 2009. This fault was causative of the 2009 M 6.3 L'Aquila earthquake. Polarization analysis was carried out after applying an antitrigger algorithm to avoid the influence of cultural activity.

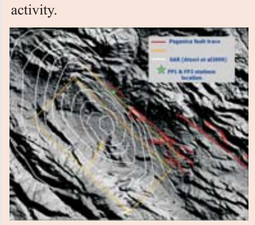

Figure 21 - Location of stations FP1 and FP2 on Paganica fault. The fault trace (red line), the fault plane projection on the horizontal plane (yellow line) and the co-seismic ground displacements (white contour lines) obtained using the differential SAR Interferometry by Atzori et al. (2009) are shown as well.

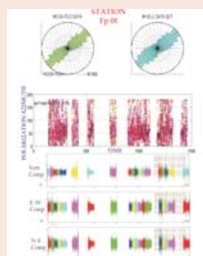

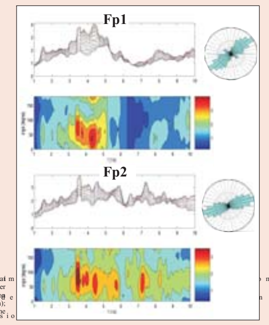

Figure 23 - HVRSs and rose diagrams for stations FP1 and FP2.

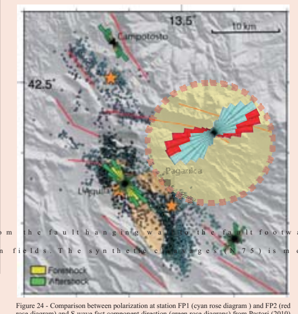

Figure 24 - Comparison between polarization at station FP1 (cyan rose diagram) and FP2 (red rose diagram) and S wave fast component direction (green rose diagrans) from Pastori (2010) obtained performing the S wave splitting analysis.at stations AQU, FAGN and CAMP (INSN network)

A marked polarization is observed at two stations across Paganica fault, that recorded ambient noise for only 40 minutes. Polarization is oriented along N50° direction, orthogonally to the fast component of S waves velocity found by Pastori et al (2010) in the area.

Conclusions

In all the study cases we have found a consistent orthogonal relation between the observed polarizations and the orientation of the predicted synthetic fracture systems. This result may be caused by the reduced stiffness in the fracture-normal direction in the damage fault zone. .
When velocity anisotropy directions are available, the horizontal ground motion polarization is consistently found to be perpendicular to the fast S wave component: this means that both fast velocity and polarization are effects of the same cause, i.e. the predominant crack orientation.

Selected references

Boness, N. L. & M. D. Zoback (2004). Stress-induced seismic velocity anisotropy and physical properties in the SAFOD Pilot Hole in Parkfield, CA. *Geophys. Res. Lett.*, **31**, L15S17, doi:10.1029/2003GL019020.
Caine, J.S., Evans, J. P., Forster, C.B. (1996). Fault zone architecture and permeability structure. *Geology,* **24**,1025-1028
Cucci, L., Pondrelli, S., Freopoli, A., Mariucci, M.T., Moro, M. (2004). Local pattern of stress field and seismogenic sources in Meandro Pergola basin and in Agri valley (Southern Italy). *Geophys. J. Int.*, **156**, 575583
Di Giulio, G., Cara, F., Rovelli, A., Lombardo, G., Rigano, R. (2009). Evidences for strong directional resonances in intensely deformed zones of the Pernicana fault, Mount Etna, Italy. *J.Geophys. Res.*, **114**, doi:10.1029/2009JB006393.
Harding, T.P & Lowell, J.D. (1979). Structural styles, their plate tectonic habitats and hydrocarbon traps in petroleum provinces, *Bull. Am. Ass. Petrol. Geol.*, **63**,10161058.
Hobbs, B.E., Means, W.D., Williams, P.P. (1976). An Outline of Structural Geology, Wiley, New York, N.Y, p. 571.
Jurkevics A. (1988). Polarization analysis of three component array data, *Bull. Seismol. Soc.Am.*, **78**, 1725-1743.
Lewis, M. & Ben Zion, Y. (2010). Diversity of fault zone damage and trapping structures in the Parkfield section of the San Andreas Fault from comprehensive analysis of near fault seismograms. *Geophys. J. Int.*, doi: 10.1111/j.1365-246X.2010.04816.x.
Pastori, M., Piccinini, D., Margheriti, L., Improta, L., Valoroso, L., Chiaraluce, L., Chiarabba, C. (2009). Stress aligned cracks in the upper crust of the Val d'Agri region as revealed by shear wave splitting. *J. Geophys. Res.,* **179**, 601614
Pastori, M. (2011). Crustal fracturing field and presence of fluid as revealed by seismic anisotropy: case histories from seismogenic areas in the Appennines. *PhD Thesis*, University of Perugia (Italy).
Riedel, W. (1929). Zur mechanik geologischer Brucherscheinungen. Zentralblatt Mineral Geol Palaont B:354368.
Spudich, P & Xu, L. (2003). Documentation of software package ISOSYN: Isochrone integration programs for earthquake ground motion calculations, CD accompanying IASPEI *Handbook of Earthquake and Engineering Seismology*, 72 pp.
Valoroso, L., Improta, L.,Chiaraluce, L.,Di Stefano, R., Ferranti, L.,Govoni, A., Chiarabba, C. (2009). Active faults and induced seismicity in the Val d'Agri area (Southern Apennines, Italy). *Geophys. J. Int.*, **178(1)**, 488502.